Stefan Hähnel, MD
Birgit Ertl-Wagner, MD
Abel-Jan Tasman, MD
Michael Forsting, MD
Olav Jansen, MD

Index terms:
Computed tomography (CT), comparative studies, 23.20
Magnetic resonance (MR), comparative studies, 23.20
Paranasal sinuses, CT, 23.12118
Paranasal sinuses, MR, 23.121412
Paranasal sinuses, surgery, 23.1267
Sinusitis, 23.25

Radiology 1999; 210:171–176

Abbreviations:
CNR = contrast-to-noise ratio
FESS = functional endoscopic sinus surgery
SNR = signal-to-noise ratio

[1] From the Departments of Neuroradiology (S.H., B.E.W., M.F., O.J.) and Otorhinolaryngology (A.J.T.), University of Heidelberg Medical School, Im Neuenheimer Feld 400, D 69120 Heidelberg, Germany. Received November 18, 1997; revision requested February 5, 1998; final revision received June 16; accepted August 20. **Address reprint requests to** S.H.

Author contributions:
Guarantors of integrity of entire study, S.H., B.E.W., O.J.; study concepts and design, S.H., O.J.; definition of intellectual content, S.H., A.J.T.; literature research, S.H., A.J.T.; clinical studies, S.H., B.E.W., M.F., O.J.; data acquisition and analysis, S.H., B.E.W., M.F., O.J.; statistical analysis, S.H.; manuscript preparation and editing, S.H., B.E.W.; manuscript review, S.H., B.E.W., O.J.

Relative Value of MR Imaging as Compared with CT in the Diagnosis of Inflammatory Paranasal Sinus Disease[1]

PURPOSE: To evaluate the relative value of magnetic resonance (MR) imaging versus computed tomography (CT) in the diagnosis of inflammatory paranasal sinus disease.

MATERIALS AND METHODS: In 30 patients suspected of having or known to have inflammation of the paranasal sinuses, both coronal CT and coronal T1-weighted, three-dimensional, gradient-echo MR imaging of the paranasal sinuses were performed. Visualization of anatomic details, kind and extent of inflammatory disease, and artifacts from dental work were scored. The scores were compared by using the Wilcoxon matched pairs signed rank test. Interexamination agreement between the two methods was calculated by using a κ analysis.

RESULTS: Most bone structures of the infundibular complex were significantly better visualized at CT than at MR imaging. Orbital and brain anatomy were visualized better at MR imaging than at CT. No artifacts from dental work occurred in diagnostically relevant regions at MR imaging. There was a substantial to almost perfect agreement between CT and MR imaging for every kind and extent of the disease except for mucosal thickening in the maxillary and frontal sinuses, in the nasal cavity, and in the infundibulum.

CONCLUSION: CT is superior to MR imaging in the depiction of fine bony details and anatomic variants and thus is superior to MR imaging in helping plan functional endoscopic sinus surgery. However, there are patient groups in which MR imaging can be used as a primary tool in screening for sinusitis.

Computed tomography (CT) in the coronal plane has become the method of choice in the evaluation of the paranasal sinuses, particularly for planning functional endoscopic sinus surgery (FESS) (1). Nevertheless, radiation exposure, artifacts from dental work, and an inconvenient prone patient position are the main limitations of paranasal sinus CT. In some patients, strictly coronal scans cannot be acquired owing to restricted extension of the neck. Some of these limitations can be avoided by using spiral CT (2).

Magnetic resonance (MR) imaging is a possible alternative to CT in the evaluation of the paranasal sinuses. The main limitations of MR imaging in the evaluation of the paranasal sinuses are a limited ability to delineate bony details and higher costs relative to CT. Moreover, patients with severe claustrophobia may not tolerate MR imaging procedures in closed-gantry systems. However, MR imaging is currently considered superior to CT in the diagnosis of intracranial and intraorbital complications of inflammatory paranasal sinus disease (1,3–5). Except for casual reports, to our knowledge, CT and MR imaging have not been directly compared by means of objective and subjective criteria to judge the diagnostic potential of each modality in inflammatory paranasal sinus disease. The purpose of our study was to evaluate objectively in a prospective study the limitations and advantages of MR imaging relative to those of CT in the diagnosis of inflammatory paranasal sinus disease.

MATERIALS AND METHODS

Thirty patients (17 women, 13 men; age range, 19–72 years) who had inflammation or were suspected of having inflammation of the paranasal sinuses were examined. To screen a

wide range of normal and pathologic variants, we examined a study group that consisted of patients who had previously undergone rhinosurgical treatment and others who had not previously undergone surgery.

The patients first underwent incremental thin-section CT scanning (PQ 2000; Picker International, Cleveland, Ohio) with the following parameters: field of view, 160 mm; section thickness, 4 mm; index, 4 mm; 100 mA; 130 kV; small focal spot; mean total acquisition time, 5 minutes. Immediately afterward, MR imaging was performed with a head coil and a 0.23-T unit (Outlook; Picker International) with an open-gantry low-field-strength system. A T1-weighted, three-dimensional, gradient-echo, fast-low-angle-shot sequence was performed with the following parameters: field of view, 240 × 250 mm; section thickness, 4 mm; no gap; flip angle, 40°; 60/12 (repetition time msec/echo time msec); 240 × 256 matrix; total scanning time, 8.6 minutes.

CT scans were obtained in the coronal plane. If a scan orientation perpendicular to the hard palate was not feasible because of reduced patient compliance, the scan orientation was approximated to the coronal plane as far as possible. The image orientation at MR imaging was adjusted to the corresponding CT scan by the orientation of anatomic landmarks in the lateral scout view. The study protocol was approved by our ethics committee. Informed consent was given by each patient.

TABLE 1
Results of the Subjective Evaluation of Anatomic Details

Structure	Average Score for CT	Average Score for MR Imaging	*P* Value	Value of MR Imaging Relative to CT*
Uncinate process				
Right	3.7	2.8	<.05	MR Imaging < CT
Left	4.2	2.9	<.05	MR Imaging < CT
Ethmoid bulla				
Right	3.9	2.5	<.05	MR Imaging < CT
Left	4.1	2.6	<.05	MR Imaging < CT
Infundibulum				
Right	3.9	2.4	<.05	MR Imaging < CT
Left	4.5	2.1	<.05	MR Imaging < CT
Middle meatus of the nasal cavity				
Right side	4.3	4.0	>.05	MR Imaging ≈ CT
Left side	4.4	3.7	>.05	MR Imaging ≈ CT
Middle concha				
Right	4.3	4.0	>.05	MR Imaging ≈ CT
Left	4.4	3.7	=.05	MR Imaging ≈ CT
Medial border of the orbit				
Right	4.7	5.0	>.05	MR Imaging ≈ CT
Left	4.7	4.9	>.05	MR Imaging ≈ CT
Bone structure of the orbital lamina				
Right	4.5	1.3	<.01	MR Imaging < CT
Left	4.6	1.4	<.01	MR Imaging < CT
Inferior border of the orbit				
Right	4.7	4.9	>.05	MR Imaging ≈ CT
Left	4.7	4.9	>.05	MR Imaging ≈ CT
Bone structure of the orbital floor				
Right	4.6	1.7	<.01	MR Imaging < CT
Left	4.6	1.7	<.01	MR Imaging < CT
Orbital fat				
Right	4.1	4.5	<.05	MR Imaging > CT
Left	4.1	4.7	<.05	MR Imaging > CT
Lateral border of the maxillary sinus				
Right	4.5	4.2	>.05	MR Imaging ≈ CT
Left	4.5	4.3	>.05	MR Imaging ≈ CT
Infraorbital foramen				
Right	3.9	2.3	<.01	MR Imaging < CT
Left	3.9	2.2	<.01	MR Imaging < CT
Alveolar recess				
Right	4.4	4.6	>.05	MR Imaging ≈ CT
Left	4.3	4.7	>.05	MR Imaging ≈ CT
Border between frontal lobe and ethmoid cells	4.8	4.7	>.05	MR Imaging ≈ CT
Bone structure of the cribriform lamina	4.6	1.5	<.01	MR Imaging < CT
Frontal lobe	2.7	5.0	<.05	MR Imaging > CT
Artifacts from dental work	3.1	1.0	<.01	MR Imaging > CT

*MR imaging ≈ CT = MR imaging and CT have the same value, MR imaging < CT = CT is superior to MR imaging, MR imaging > CT = MR imaging is superior to CT.

Objective Evaluation

On both CT and MR images, different regions of interest were defined within the lesions of the paranasal sinuses and the nasal cavity, within the medial rectus muscle, within the orbital fat, and within the air outside the head. Signal-to-noise ratio (SNR) of the lesions (SNR_l), contrast-to-noise ratio (CNR) of the lesions (CNR_l), and CNR of the medial rectus muscle (CNR_m) were calculated for every CT and MR image.

For the MR images, the ratios were calculated as $SNR_l = SI_l/SD_b$, $CNR_l = (SI_l - SI_b)/SD_b$, and $CNR_m = (SI_f - SI_m)/SD_b$, where SI_l is the signal intensity of the lesion, SD_b is the SD of the signal intensity of the air outside the head (background noise), SI_f is the signal intensity of the orbital fat, SI_m is the signal intensity of the medial rectus muscle, and SI_b is the signal intensity of the air outside the head.

For the CT images, the ratios were calculated as $SNR_l = HU_l/SD_b$, $CNR_l = (HU_l - HU_b)/SD_b$, and $CNR_m = (HU_m - HU_f)/SD_b$, where HU_l is the Hounsfield unit of the lesion, SD_b is the SD of the attenuation of the air outside the head (background noise), HU_f is the Hounsfield unit of the orbital fat, HU_m is the Hounsfield unit of the medial rectus muscle, and HU_b is the Hounsfield unit of the air outside the head.

Mean values were calculated for SNR_l, CNR_l, and CNR_m. The Wilcoxon matched pairs signed rank test was used to test for significant differences between CT and MR imaging, and a *P* value less than or equal to .05 was considered to indicate a statistically significant difference.

Subjective Evaluation

For qualitative assessment, both CT and MR images were evaluated subjectively by two neuroradiologists (S.H., B.E.W.) with regard to the following criteria.

1. Delineation of the infundibular complex (uncinate process, ethmoid bulla, infundibulum, Haller cell, middle meatus of the nasal cavity), parainfundibular complex (middle concha, agger nasi cell), orbital anatomy (medial border of the orbit, inferior border of the orbit, orbital fat), lateral borders of the maxillary sinus, alveolar recess, infraorbital foramen, and the border between the frontal lobe and ethmoid cells. These structures are delineated either by the direct visualization of the corresponding bone structures, if possible, or by the contrast between two adjacent compartments containing differ-

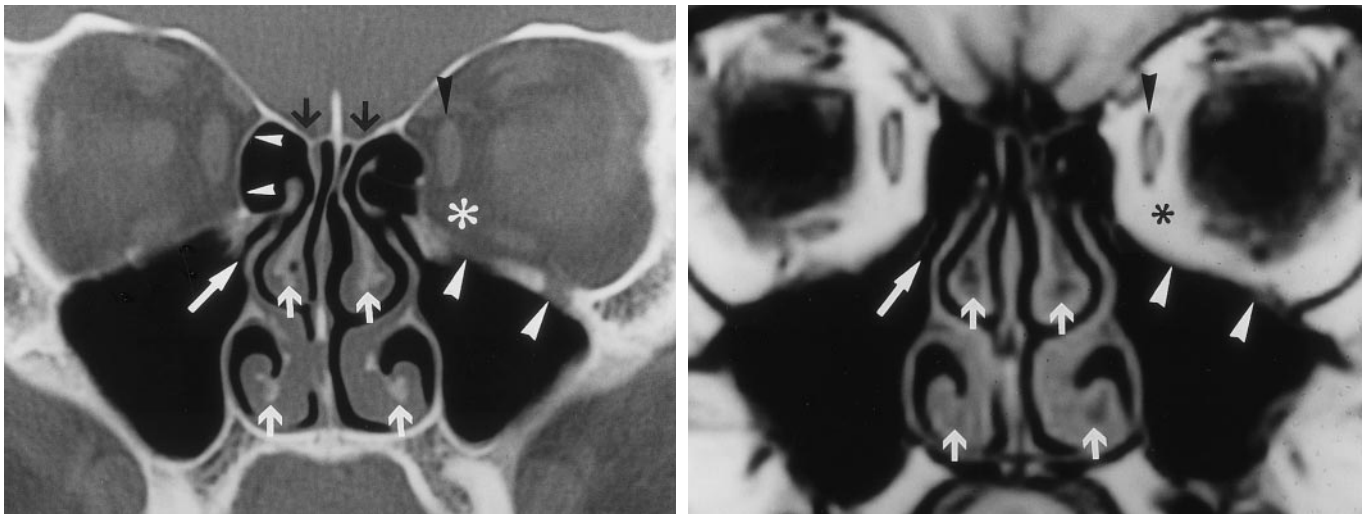

a. **b.**

Figure 1. Images obtained in a 36-year-old woman with planned heart valve implantation who was examined for inflammatory paranasal disease. **(a)** CT scan depicts the anatomy of the infundibular (large white arrow) and parainfundibular complex very well. The bone structures of the inferior and middle conchae (small white arrows), the orbital lamina (small white arrowheads), the orbital floor (large white arrowheads), and the cribriform lamina (black arrows) are clearly delineated. Contrast between orbital fat (*) and the medial rectus muscle (black arrowhead) is moderate. Inflammatory disease is not present. **(b)** MR image (60/12; flip angle, 40°) shows moderately delineated infundibular (large arrow) and parainfundibular complex. The bone structures of the inferior and middle conchae (small arrows) are visible. The bone structures of the orbital lamina, of the orbital floor, and of the cribriform lamina are not delineated. However, the medial and inferior (white arrowheads) borders of the orbit, the border between the frontal lobe and ethmoid cells, and the borders of the maxillary sinuses are clearly seen. Contrast between orbital fat (*) and the medial rectus muscle (black arrowhead) is excellent.

ent material (fat, brain, soft tissue, mucosa, or mucus).

For instance, the medial border of the orbit can be delineated either by means of visualization of the bone structure of the orbital lamina or by means of contrast between the orbital fat and the material within the ethmoid cells (air, mucus); the uncinate process can be delineated either by means of visualization of the bone structure of the uncinate process or by means of contrast between the mucosal layer of the uncinate process and the surrounding air.

2. Visualization of the bone structure of the orbital lamina, the bone structure of the orbital floor, and the bone structure of the cribriform lamina as structures with areas of bone attenuation on CT scans or areas of low signal intensity on MR images. Detecting these bone structures directly is important for planning FESS.

3. The kind and extent of the disease—mucosal thickening, partial obstruction by cystic or polypoid lesions, partial obstruction by noncystic or nonpolypoid lesions, or total obstruction. 4. Artifacts from dental work in diagnostically relevant regions.

Both neuroradiologists were blinded to the clinical history of the patients, and neither had performed any of the imaging procedures himself or herself. Each of the neuroradiologists had previously assessed more than 300 coronal CT scans in patients with paranasal sinus disease. To assess the visualization of anatomic details and of the kind and extent of the disease, scoring was based on a five-point scale as follows: ''1'' indicated nonvisualization; ''2,'' very poor visualization; ''3,'' indeterminate visualization; ''4,'' fairly good visualization; and ''5,'' definite visualization. Artifacts from dental work in diagnostically relevant regions were scored on a five-point scale as well: ''1'' indicated no artifact in any diagnostically relevant region; ''2,'' few artifacts in diagnostically relevant regions; ''3,'' moderate artifacts in diagnostically relevant regions; ''4,'' marked artifacts in diagnostically relevant regions; and ''5,'' extreme artifacts in diagnostically relevant regions.

The final score was based on a consensus between the two raters. Scores were calculated separately for structures on the right-hand side and those on the left-hand side, because the anatomy of the paranasal sinuses may differ between the sides, especially in patients who had previously undergone rhinosurgical intervention. An average score for both CT and MR imaging was calculated for each criterion, and the differences between CT and MR imaging were tested by using the Wilcoxon matched pairs signed rank test. A P value less than or equal to .05 was considered to indicate a statistically significant difference.

Interexamination agreement for anatomic variants (concha bullosa, agger nasi cell, Haller cell) and for the kind and extent of the disease was calculated by using squared weighted κ coefficients. According to Landis and Koch (6), a κ coefficient of less than 0.00 indicated poor agreement; a κ coefficient of 0.01–0.20, slight agreement; a κ coefficient of 0.21–0.40, fair agreement; a κ coefficient of 0.41–0.60, moderate agreement; a κ coefficient of 0.61–0.80, substantial agreement; and a κ coefficient of 0.81–1.00, almost perfect agreement.

RESULTS

Evaluation of CT images revealed paranasal inflammatory disease (mucosal thickening, partial obstruction by cystic or polypoid lesions, partial obstruction by noncystic or nonpolypoid lesions, or total obstruction) in the frontal sinus in 17 patients (57%), the ethmoid sinus in 19 patients (63%), the sphenoid sinus in 11 patients (37%), the right maxillary sinus in 18 patients (60%), the left maxillary sinus in 18 patients (60%), and the nasal

cavity in 30 patients (100%). Mucosal thickening in the right infundibulum was found in 13 patients (43%) and in the left infundibulum in 11 patients (37%). Seven patients did not show any signs of inflammatory disease except mucosal thickening in the nasal cavity.

Objective Evaluation

SNR_l was significantly higher for MR imaging than for CT (27.6 vs 2.0, $P < .001$). As expected, CNR_l was significantly higher for CT than for MR imaging (50.4 vs 24.3, $P < .001$). CNR_m was significantly higher for MR imaging than for CT (22.6 vs 6.5, $P < .001$). The latter was in good agreement with the subjective finding that the fat between the medial rectus muscle and the orbital lamina was better visualized at MR imaging than at CT (Table 1, Fig 1).

Subjective Evaluation

The statistical analysis always led to the same level of significance for both sides in every structure, so the two sides of each structure will be discussed together rather than separately. The following anatomic details were visualized significantly better at CT than at MR imaging: uncinate process, ethmoid bulla, infundibulum, bone structure of the orbital lamina, bone structure of the orbital floor, infraorbital foramen, and bone structure of the cribriform lamina (Table 1).

No statistically significant differences between CT and MR imaging were found in the visualization of the middle concha, the alveolar recess, the lateral borders of the maxillary sinus, the middle meatus of the nasal cavity, the medial and inferior borders of the orbit, and the border between frontal lobe and ethmoid cells (Table 1).

MR imaging was significantly superior to CT in the visualization of the fat between the medial rectus muscle and the medial border of the orbit, and of the frontal lobe. Artifacts were significantly more pronounced on CT scans than on MR images; in MR imaging, no artifacts occurred in diagnostically relevant regions (Table 1).

Evaluation of κ-based interexamination agreement revealed only poor to fair agreement in the detection of anatomic variants (Table 2). There was substantial to almost perfect agreement between CT and MR imaging for every kind and extent of the disease except for mucosal thickening in the maxillary and frontal sinuses, the nasal cavity, and the infundibulum (Table 3).

DISCUSSION

Our prospective study directly compares CT and T1-weighted MR imaging in the evaluation of inflammatory paranasal sinus disease. The current opinion is that CT is superior to MR imaging in screening for inflammatory paranasal sinus disease, particularly for planning FESS (1,3–5). However, this opinion is based solely on general experience and casual reports. FESS is indicated only in patients who have severe or repeated bouts of bacterial sinusitis that respond only briefly to antibiotics, in patients with chronic hyperplastic sinusitis, in patients with mucoceles, and in patients with periorbital cellulitis caused by ethmoiditis (1).

We found a frequency of inflammatory paranasal disease of up to 63% (19 of 30 patients) depending on the affected sinus. This frequency is higher than the prevalence of inflammatory paranasal disease because the patient population in our study was preselected. However, the frequency of the disease we found is higher than that reported by others (7) in larger, preselected patient populations. An explanation for the higher frequency of disease in our study compared with that in the literature could be the small size of our patient group.

According to Sonkens et al (7), there are five patterns of inflammatory paranasal sinus disease: (*a*) In the infundibular pattern, disease is limited to the infundibulum and the adjacent maxillary sinus; the frontal and ethmoid sinuses are normal. Pathophysiologic causes for this pattern are swollen mucosa, polypoid lesions, and Haller cells. Infundibulotomy is the therapeutic method of choice and produces excellent results in most cases. (*b*) In the ostiomeatal unit pattern, the middle meatus of the nasal cavity and, secondarily, the adjacent anterior and middle ethmoid cells and the maxillary and frontal sinuses are involved. Pathophysiologic causes for this pattern are swollen mucosa, polypoid lesion, concha bullosa, septal deviation, and nasal tumor. Infundibulotomy in combination with ethmoid bullectomy is often required. (*c*) In the sphenoethmoidal recess pattern, the sphenoid sinus and, to a lesser extent, the ipsilateral posterior ethmoid cells are involved. The level of obstruction is within the sphenoethmoidal recess. (*d*) In the sinonasal polyposis pattern, polypoid lesions fill the nasal cavity and the sinuses bilaterally. In effect, this is a mixture of the previously mentioned patterns *a*, *b*, and *c*. (*e*) In the sporadic (unclassifiable) pattern, the extent of the disease does not appear to be related to the known mucous drainage patterns, and there may be retention cysts, mucoceles, and postsurgical changes.

The extent of the disease according to one of these five patterns is of special interest for the otorhinolaryngologist plan-

TABLE 2
Agreement between CT and MR Imaging in the Visualization of Anatomic Variants of the Paranasal Sinuses

Location	κ Value*
Concha bullosa	
Right side	0.11
Left side	0.17
Agger nasi cell	
Right side	0.03
Left side	0.23
Haller cell	
Right side	0.13
Left side	0.22

*κ value = squared weighted κ coefficient.

TABLE 3
Agreement between CT and MR Imaging in the Evaluation of Kind and Extent of Inflammatory Paranasal Sinus Disease

Morphologic Type	κ Value*
Frontal sinus	
Cystic or polypoid lesion†	0.90
Noncystic or nonpolypoid lesion†	0.93
Mucosal thickening	0.44
Total obstruction	0.90
Ethmoid sinus	
Cystic or polypoid lesion†	1.00
Noncystic or nonpolypoid lesion†	0.97
Mucosal thickening	0.93
Total obstruction	1.00
Sphenoid sinus	
Cystic or polypoid lesion†	1.00
Noncystic or nonpolypoid lesion†	0.78
Mucosal thickening	0.76
Total obstruction	0.99
Right maxillary sinus	
Cystic or polypoid lesion†	0.93
Noncystic or nonpolypoid lesion†	1.00
Mucosal thickening	0.35
Total obstruction	1.00
Left maxillary sinus	
Cystic or polypoid lesion†	0.97
Noncystic or nonpolypoid lesion†	0.91
Mucosal thickening	0.50
Total obstruction	0.62
Nasal cavity	
Cystic or polypoid lesion†	0.62
Noncystic or nonpolypoid lesion†	0.62
Mucosal thickening	0.34
Total obstruction	0.97
Right infundibular mucosal thickening	0.10
Left infundibular mucosal thickening	0.20

*κ value = squared weighted κ coefficient.
† Partial obstruction.

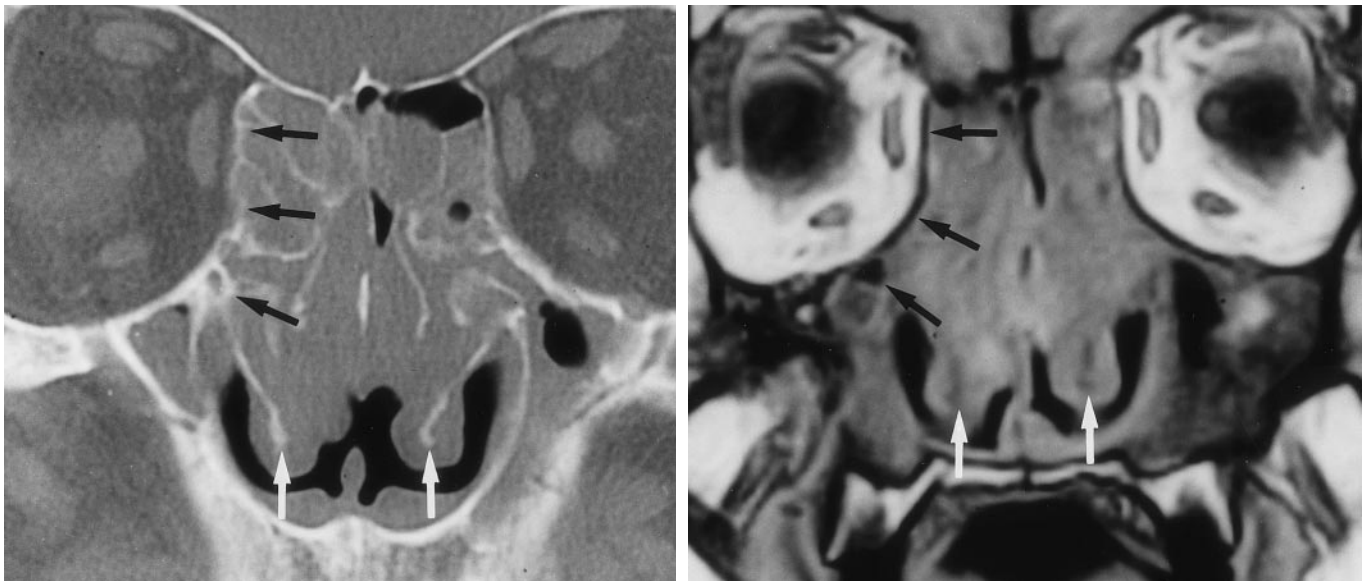

a. **b.**

Figure 2. Images obtained in a 49-year-old man suspected of having nasal polyposis. **(a)** CT scan shows that despite nearly total opacification of the middle meatus and the ethmoid cell system, the bone structures of the inferior (white arrows) and middle conchae, the ethmoid cells, and the orbital lamina (black arrows) are excellently delineated. **(b)** MR image (60/12; flip angle, 40°) does not depict the fine bone structures of the middle concha and the ethmoid cells. Visualization of the bone structure of the inferior concha (white arrows) is indeterminate. The bone structure of the orbital lamina (black arrows) is clearly seen as loss of signal intensity, because the adjacent sinuses are filled with material containing water (mucus or mucosa).

ning a therapeutic intervention, such as FESS. The visualization of anatomic details of the paranasal sinuses is necessary, particularly when planning FESS (8). In accordance with the findings of Mafee et al (1) and Zinreich (5), we found that CT is superior to MR imaging in the delineation of fine bone structures of the infundibular complex; of the bone structures of the orbital lamina, of the orbital floor, and of the cribriform lamina; and of the following anatomic variants: concha bullosa, agger nasi cell, and Haller cell. Thus, CT is superior to MR imaging in planning FESS. At MR imaging, the bone structures of the orbital lamina, of the orbital floor, and of the cribriform lamina could be detected as structures with low signal intensity only if the adjacent sinuses (ethmoid cells, maxillary sinuses) were obstructed (Fig 2). However, the intraorbital anatomy was visualized better at MR imaging than at CT. The kind and the extent of the inflammatory disease were evaluated almost equally well with both modalities. Retrospective evaluation of the κ tables and the images revealed that in some cases where mucosal thickening of the frontal sinus was definitely visualized at CT, this mucosal thickening was confused with the fat of the diploë on MR images. However, in many cases in which MR imaging was able to definitely depict whether there was mucosal thickening in the maxillary sinus (Fig 3), the nasal cavity, or the infundibulum, CT had to be judged indeterminate because of artifacts from dental work.

To depict orbital or intracranial complications of the disease or the rhinosurgical intervention, the optimal modality has to depict the orbital and frontal lobe anatomy and to show the anatomy of the ethmoid cells, the border between the frontal lobe and ethmoid cells (low-lying cribriform lamina), and the orbital borders. Our study showed that MR imaging is superior to CT in the depiction of the orbital anatomy and, thus, in the evaluation of orbital complications both of the actual sinus infection and of FESS. For the evaluation of intracranial complications, however, T2-weighted images and contrast material–enhanced T1-weighted images ought to be obtained in addition to the T1-weighted non–contrast material–enhanced images exclusively used in our study. We found that the orbital borders and the border between the frontal lobe and ethmoid cells can be visualized almost equally well at CT and at MR imaging.

In the Department of Neuroradiology, University of Heidelberg, indications for paranasal sinus CT are as follows: (*a*) Suspected or known inflammation of the paranasal sinuses and the intention of performing FESS (approximately 65%). (*b*) Screening for inflammation of the paranasal sinuses before implantation of organs or prostheses (approximately 10%). (*c*) Suspected complications of sinus infection, such as orbital or brain abscess (approximately 10%). (*d*) Screening for foci of septic disease (approximately 5%). (*e*) Suspected complications of FESS, such as orbital or brain injury (approximately 5%). (*f*) Other suspected disease of the paranasal sinuses (eg, choanal atresia [approximately 5%]).

Whenever FESS is planned in a patient, CT ought to be used as a primary diagnostic tool. However, we believe that MR imaging could be used as a primary diagnostic tool in screening for inflammatory paranasal sinus disease in patients in the following circumstances: (*a*) Screening for foci of septic disease or before implantation of organs (eg, bone marrow, kidney) or prostheses (eg, heart valve). Particularly in young people, primarily MR imaging should be used to avoid radiation exposure. (*b*) Screening and follow-up of orbital complications of sinus infection or FESS. (*c*) Evaluating paranasal sinus disease in patients with dental implants. Anatomic details of the alveolar recess of the maxillary sinus, of the nasal cavity, and sometimes of the orbital fat are better visualized at MR imaging in patients with dental implants.

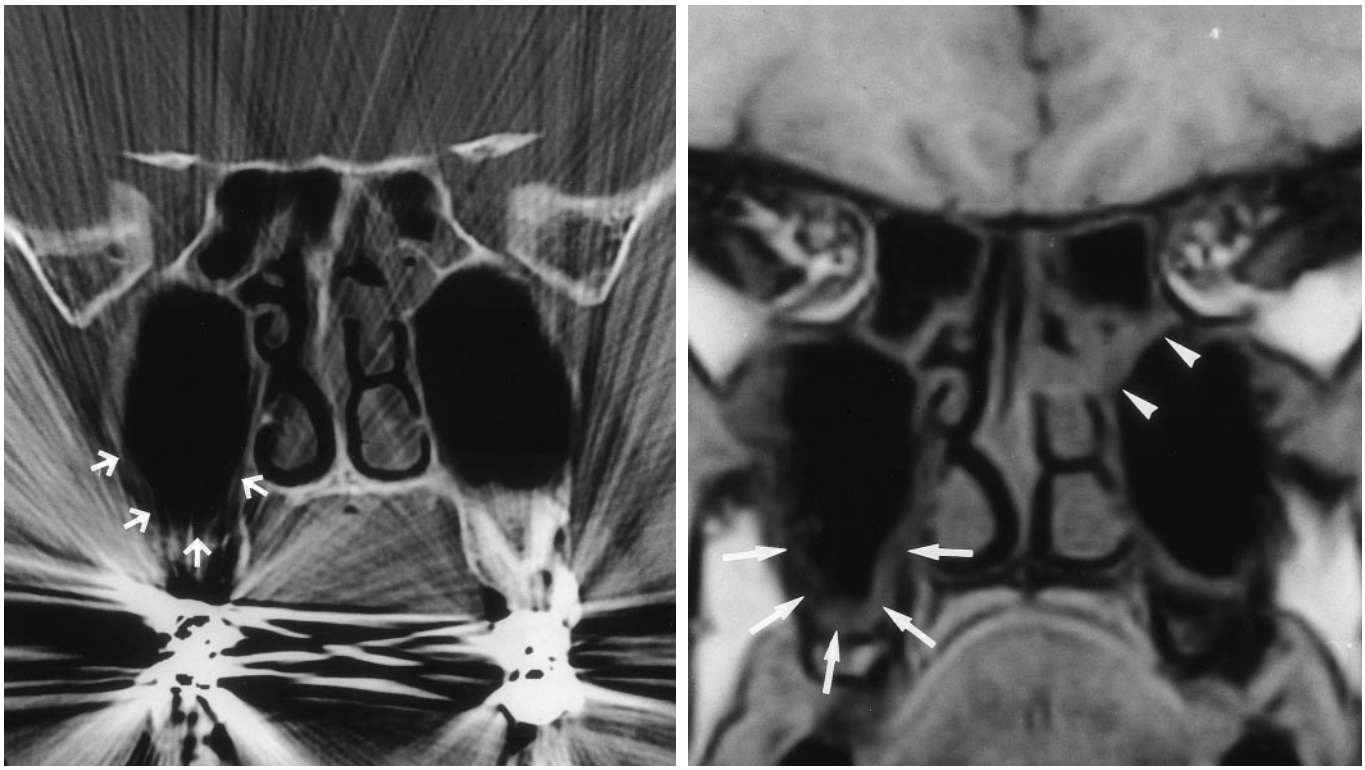

a. **b.**

Figure 3. Images obtained in a 38-year-old man suspected of having chronic inflammatory disease of the maxillary sinus. **(a)** CT scan shows extreme artifacts from dental work. Mucosal thickening (arrows) in the right maxillary sinus can easily be missed. Evaluation of the frontal lobe and the orbital tissues is almost impossible, even if a soft-tissue window were used. Partial opacification of the ethmoid cells is present. **(b)** MR image (60/12; flip angle, 40°) depicts mucosal thickening (arrows) in the right maxillary sinus very well. The frontal lobe and orbits can be evaluated very well. Soft-tissue signal intensity in the ethmoid cells (arrowheads) is present.

Some patients examined primarily by means of MR imaging may have to be examined by means of CT as well if FESS is indicated at the MR imaging examination (eg, in patients with periorbital cellulitis from ethmoiditis or mucoceles). Furthermore, MR imaging might be used to assess therapeutic success in inflammatory disease without any radiation exposure.

To keep examination times and costs of MR imaging comparable to those of standard sinus CT, we acquired only T1-weighted MR images. The MR sequence chosen had to provide high spatial resolution for detailed visualization of the anatomy of the paranasal sinuses; a high SNR; and an acquisition time comparable to that of CT, meaning less than 10 minutes. The results of our own pilot study revealed that, although the signal intensity of the sinus lesions was higher, the overall SNR of T2*-weighted and T2-weighted fast spin-echo sequences was lower and image quality was poorer than those of the T1-weighted sequence.

Som et al (9) found that there is loss of the MR image signal intensity of paranasal sinus lesions at protein concentrations of more than 40% on T1-weighted images and at protein concentrations of more than 30% on T2-weighted images. Thus, the range for depicting lesions is higher on T1-weighted than on T2-weighted images.

In conclusion, our comparison of CT and MR imaging in the examination of patients with inflammatory paranasal sinus disease confirms the current opinion that CT is superior to MR imaging in helping plan FESS. However, we believe that MR imaging can be used as a primary diagnostic tool in the diagnosis of inflammatory paranasal sinus disease in screening for foci of septic disease, before implantation of organs or prostheses, in the diagnosis of complications of sinus infection or FESS, and in patients with dental implants. Furthermore, MR imaging might be used to help assess therapeutic success in patients with inflammatory disease, with the advantage of avoiding radiation exposure to the patients.

Acknowledgment: For technical support, we thank Klaus Kotitschke, PhD, Picker International, Hofheim-Wallau, Germany.

References

1. Mafee MF, Chow JM, Meyers R. Functional endoscopic sinus surgery: anatomy, CT screening, indications, and complications. AJR 1993; 160:735–740.
2. Suojanen JN, Regan F. Spiral CT of the paranasal sinuses. AJNR 1995; 16:787–789.
3. Mafee MF. Modern imaging of paranasal sinuses and the role of limited sinus computerized tomography: considerations of time, cost and radiation. Ear Nose Throat J 1994; 73:532–546.
4. Hasso AN, Lambert D. Magnetic resonance imaging of the paranasal sinuses and nasal cavities. Top Magn Reson Imaging 1994; 6:209–223.
5. Zinreich SJ. Paranasal sinus imaging. Otolaryngol Head Neck Surg 1990; 103:863–869.
6. Landis JR, Koch GG. The measurement of observer agreement for categorical data. Biometrics 1977; 33:159–174.
7. Sonkens JW, Harnsberger HR, Blanch GM, Babbel RW, Hunt S. The impact of screening sinus CT on the planning of functional endoscopic sinus surgery. Otolaryngol Head Neck Surg 1991; 105:802–813.
8. Kaluskar SK, Patil NP, Sharkey AN. The role of CT in functional endoscopic sinus surgery. Rhinology 1993; 31:49–52.
9. Som PM, Dillon WP, Fullerton GD, Zimmerman RA, Rajagopalan B, Marom Z. Chronically obstructed sinonasal secretions: observations on T1 and T2 shortening. Radiology 1989; 172:515–520.